Pharmacological modulation of septins restores calcium homeostasis and is neuroprotective in models of Alzheimer's disease

Authors: Katrien Princen[1]†, Tom Van Dooren[1]†‡, Marit van Gorsel[1], Michael Dumbacher[1], Nikolaos Louros[2,3], Ilse Bastiaens[1], Xiaojuan Wang[4], Kristel Coupet[1], Shana Dupont[1], Eva Cuveliers[1], Annick Lauwers[1], Mohamed Laghmouchi[1], Thomas Vanwelden[1], Sofie Carmans[1], Nele Van Damme[1], Hein Duhamel[1], Seppe Vansteenkiste[1], Jovan Prerad[1], Karolien Pipeleers[1], Olivier Rodiers[1], Liese De Ridder[1], Sofie Claes[1], Yoni Busschots[1], Lentel Pringels[1], Vanessa Verhelst[1], Eveline Debroux[1], Marinka Brouwer[5], Sam Lievens[6,7]§, Jan Tavernier[6,7]§, Melissa Farinelli[8], Sandrine Hughes-Asceri[8], Marieke Voets[1], Joris Winderickx[1,9], Stefaan Wera[1], Joris de Wit[5], Wim Anneart[4], Joost Schymkowitz[2,3], Frederic Rousseau[2,3], Henrik Zetterberg[10,11,12,13,14], Jeffrey L Cummings[15], Tom Cornelissen[1], Hans De Winter[16], Koen De Witte[1], Marc Fivaz[1]* and Gerard Griffioen[1]*.

[1]reMYND NV; Bio-Incubator, Gaston Geenslaan 1, Leuven-Heverlee 3001, Belgium.
[2]Switch Laboratory, VIB Center for Brain and Disease Research, Herestraat 49, 3000 Leuven, Belgium.
[3]Switch Laboratory, Department of Cellular and Molecular Medicine, KU Leuven, Herestraat 49, 3000 Leuven, Belgium.
[4] Laboratory for membrane trafficking, VIB-Center for Brain and Disease Research & Dept. Neurosciences, Herestraat 49, 3000 Leuven, Belgium.
[5]
[6]Cytokine Receptor Lab; VIB Department of Medical Protein Research, Ghent, Belgium.
[7]Department of Biochemistry, Ghent University, Ghent, Belgium.
[8] E-PHY-SCIENCE ; Bioparc Sophia-Antipolis, 2400 route des Colles, 06410 Biot, France.
[9]Functional Biology, Department of Biology, KU Leuven, Kasteelpark Arenberg 31, Leuven-Heverlee 3001, Belgium
[10]Department of Psychiatry and Neurochemistry, Institute of Neuroscience and Physiology, the Sahlgrenska Academy at the University of Gothenburg; Mölndal, Sweden.
[11]Clinical Neurochemistry Laboratory, Sahlgrenska University Hospital; Mölndal, Sweden.
[12]Department of Neurodegenerative Disease, UCL Institute of Neurology; Queen Square, London, UK.
[13]UK Dementia Research Institute at UCL; London, UK
[14]Hong Kong Center for Neurodegenerative Diseases; Clear Water Bay, Hong Kong, China
[15]Department of Brain Health; School of Integrated Health Sciences, University of Nevada Las Vegas (UNLV).
[16]Department of Pharmaceutical Sciences, University of Antwerp, Belgium

†equal contribution

‡present address: UCB Biopharma SRL; chemin du Foriest B-1420 Braine-l'Alleud, Belgium.

§present address: Orionis Biosciences; Ghent, Belgium.

¶present address: VIB Discovery Sciences, Bio-Incubator; Gaston Geenslaan 1, 3001 Leuven, Belgium.

*Corresponding authors. Email: marc.fivaz@remynd.com and gerard.griffioen@ext.remynd.com

Abstract

Deviant calcium signaling is a central pathological component of Alzheimer's disease (AD). Here, we describe the identification of a novel class of compounds – ReS19T – that restore calcium homeostasis in cell-based models of tau pathology. Diseased tau leads to uncontrolled activation of store-operated calcium channels (SOCCs) by causing disassembly of septin filaments. Binding of ReS19T to septin 6 restores filament polymerization in the disease state and restrains calcium entry through SOCCs. In amyloid-β and tau-driven disease models, ReS19T restored synaptic plasticity, improved neuronal survival and attenuated the development of both amyloid-β and tau pathology. Hence, neurotoxic cytosolic calcium is both a cause and consequence of AD pathology. Our findings provide support for calcium-driven neurodegeneration and identify septin 6 as a promising therapeutic target to correct calcium dysfunction in AD.

One-Sentence Summary

Restoring calcium homeostasis by modulation of septin 6 is neuroprotective in models of Alzheimer's disease.

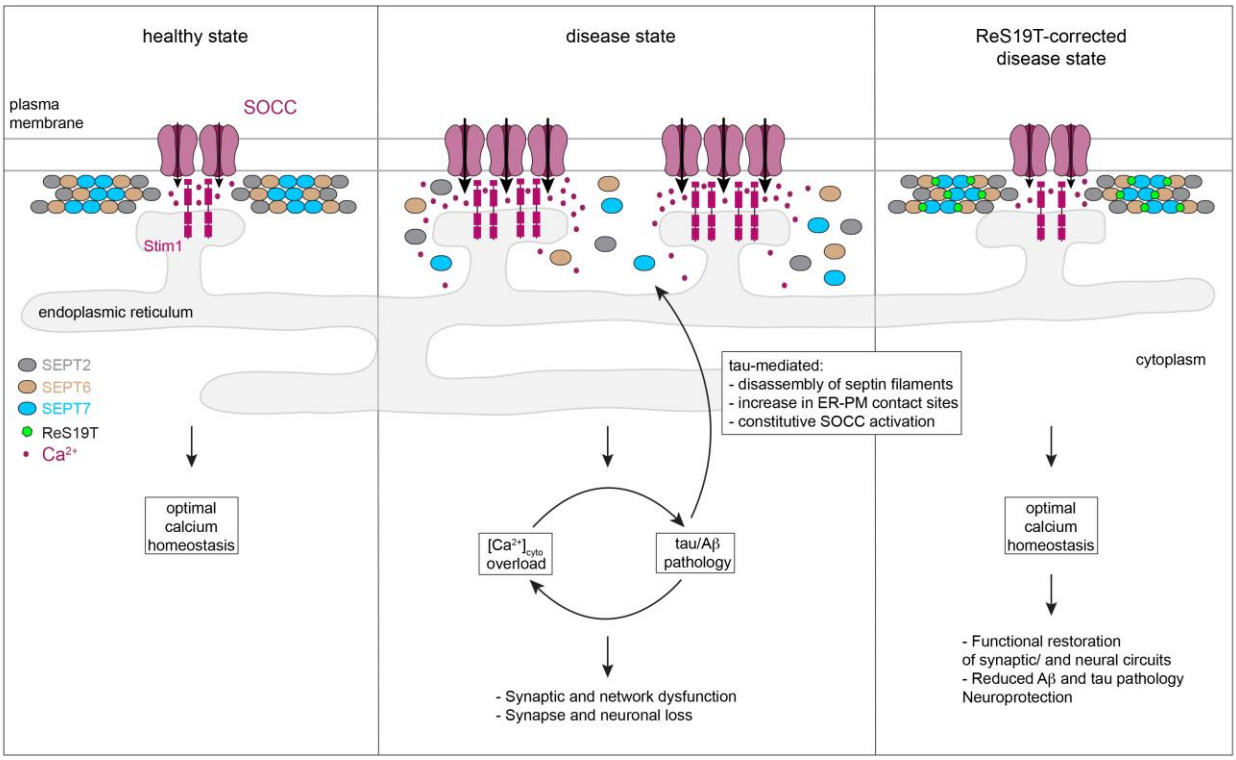

Graphical abstract. ReS19T mechanism of action. In the disease state, tau pathology disrupts septin filament assembly causing aberrant (store-independent) activation of Store-Operated Calcium Channels (SOCCs). Constitutive activation of SOCCs leads to a prolonged rise in cytoplasmic calcium levels setting off a series of self-amplifying pathophysiological events. By binding at the interface of septin filaments, ReS19T restores their assembly at the cell cortex, where they prevent spurious activation of SOCCs, thus restoring calcium homeostasis, neural circuit connectivity, and preventing neuronal loss.

Alzheimer's disease (AD) is the main cause of dementia afflicting over 40 million people worldwide (*1*). With no cure and few approved therapies, AD is fast becoming one of the most expensive and devastating diseases of this century. Therefore, there is an urgent need to accelerate development of therapeutics that target the root cause of neurodegeneration in AD.

Deranged calcium signaling is increasingly recognized as a proximal and central pathological event in AD and other types of dementia. Sustained disturbances in calcium signaling occur in the preclinical phase of the disease, before the development of overt symptoms (*2–5*) and trigger synapse disruption (*6, 7*), a key pathological event that underlies memory impairment and precedes neuronal death (*8*). Calcium dysregulation in AD is multiform and complex, but ultimately manifests with sustained elevation of cytoplasmic calcium levels $[Ca^{2+}]_{cyto}$ in both familial and idiopathic forms of the disease (*9, 10*).

In diseased neurons, elevated resting $[Ca^{2+}]_{cyto}$ contributes to the development of AD pathology including the production of pathological Aβ and tau species. Reciprocally, AD pathological changes cause elevation in resting $[Ca^{2+}]_{cyto}$, which executes a program of neurodegeneration initiated by synaptic disruption and culminating with the activation of neuronal death pathways (*11–14*). This suggests that deregulated $[Ca^{2+}]_{cyto}$ fuels a self-reinforcing amplification of AD pathobiology ultimately causing neuronal demise.

A variety of calcium channels and signaling systems are malfunctioning in AD, ranging from increased activity of N-methyl-D-aspartate (NMDA) receptors (*15*) and voltage-gated calcium channels (VGCCs) (*16*) at the synapse, to impaired mitochondrial calcium buffering (*17*) and exaggerated calcium release from the endoplasmic reticulum (ER) – an effect mediated by upregulation of inositol-3-phosphate (*18*) and ryanodine (*6*) receptors. Linked to disturbances in ER calcium homeostasis, store-operated calcium entry (SOCE), a calcium influx pathway activated by depletion of calcium from ER stores, has also been implicated in AD. Intriguingly, SOCE is downregulated by several familial AD mutations in presenilin-1 (PS1), but stimulated by others, depending on the impact of these mutations on ER calcium leakage (*10*). Moreover, an excess of tau exacerbates SOCE (*19*), while this calcium influx pathway promotes activation of the inflammasome in the disease state (*20*), hinting at a context-specific influence of SOCE in AD.

Calcium dysfunction in AD is therefore a promising therapeutic target, faced however, with one significant challenge: interventions that interfere with physiological calcium signaling events are likely to have adverse consequences on synaptic networks and cognitive performance and may affect non-neurologic organ systems. Here we report the identification and characterization of a novel class of compounds – ReS19T – that circumvent this problem by selectively targeting an aberrant form of SOCE triggered by pathological tau, without impacting synaptic and receptor-mediated Ca^{2+} signaling in physiological conditions. ReS19T compounds efficiently cross the blood-brain barrier, rescue synaptic and cognitive deficits in AD mouse models, and reduce the abundance of Aβ and tau pathology.

ReS19T: a small molecule scaffold that restores calcium homeostasis and neutralizes Tau- and Aβ-driven neurotoxicity

To discover new potential AD targets and corresponding therapeutics, we developed a cell-based screening assay that recapitulates tau- and Ca^{2+}-induced toxicity in neuroblastoma cells (*21*). This assay involves stable expression of human tau with a pathological mutation (P301L) associated with frontotemporal dementia (FTD) and causing aggressive tau hyper-phosphorylation and

aggregation (*22*), in combination with chronic exposure to all trans-retinoic acid (ATRA), an inducer of neuronal differentiation. In this context, tauP301L causes extensive cell death, compared to wild-type (wt) tau, or no transgene expression (Fig. S1A). Previous characterization of this assay revealed that toxicity is associated with elevation of cytoplasmic calcium $[Ca^{2+}]_{cyto}$ and that interventions lowering $[Ca^{2+}]_{cyto}$ efficiently rescue cell death, indicating calcium-driven tau neurotoxicity (*21*).

Screening of an in-house compound library led to the identification of several hits that alleviate $[Ca^{2+}]_{cyto}$ overload and toxicity (Figs. 1A and S1B). We focused on a thiadiazole derivative for further development. After multiple rounds of structure-activity optimization, we obtained a series of compounds with a common scaffold (ReS19T) that efficiently counteract toxicity and restore normal $[Ca^{2+}]_{cyto}$ with EC50s in both assays between 15 and 20 nM (Fig. 1A). ReS19T had no effect on tau expression or ATRA-dependent gene transcription (Fig. S1C,D). Neurotoxic soluble amyloid oligomers (Aβ-derived diffusible ligands, ADDLs ref) induce a sustained increase in neuronal $[Ca^{2+}]_{cyto}$. To test whether ReS19T rescues ADDL-induced synaptic loss and neuronal toxicity, we treated rat hippocampal neurons with purified ADDLs in the presence of ReS19T or vehicle. ReS19T restored dendritic spine density (Figs. 1B,C) and fully rescued neurons from ADDL-induced cell death (Fig. 1D), demonstrating that both tau- and Aβ-induced neurotoxicity are countered by the compound in cell-based assays.

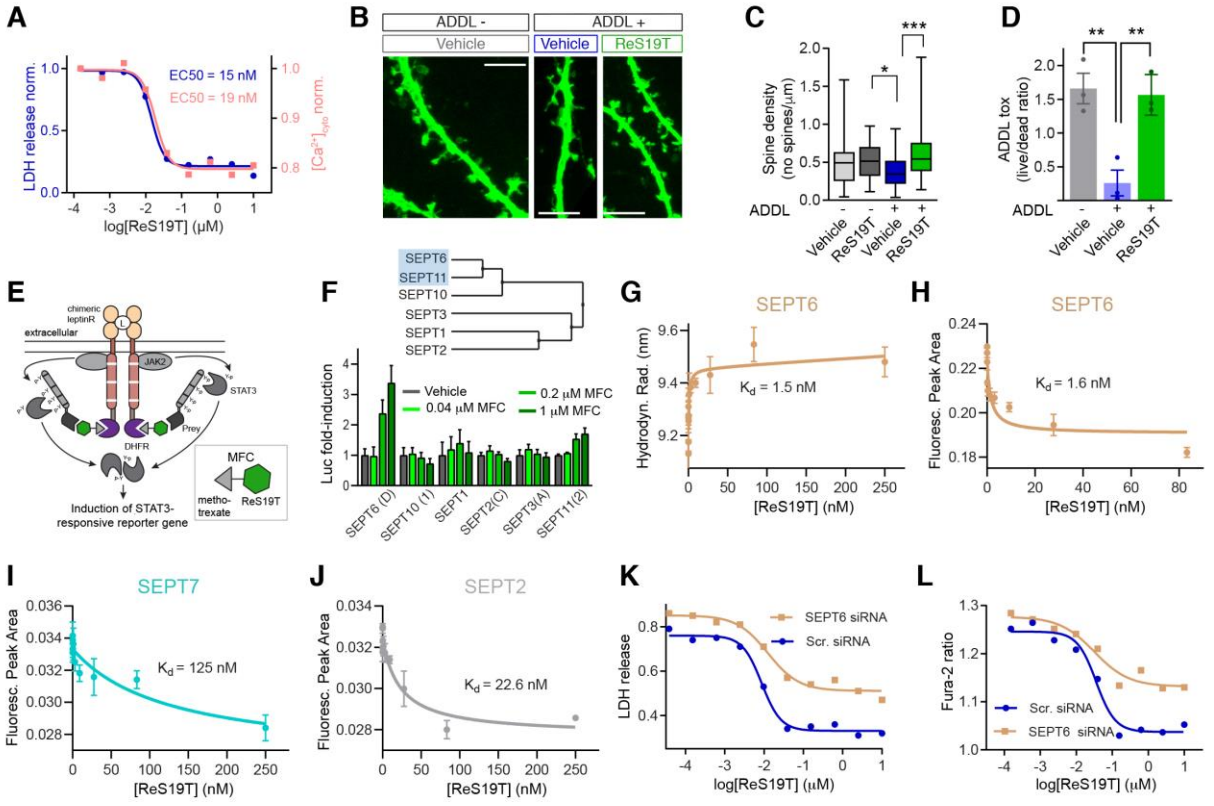

Fig. 1 Identification of ReS19T and its target. (A) Cell death and elevated $[Ca^{2+}]_{cyto}$ in ATRA-treated tauP301L-expressing BE(2)-M17 cells are mitigated by ReS19T-127 in the low nM range. (B-D) Rat hippocampal neurons (DIV 22) treated with vehicle or ReS19T-127 (240 nM) and exposed (or not) to ADDL (0.5 μM) (B,C) or ADDL (1 μM) (D) for 24 hrs. (B,C) Dendritic spine density measured in dendritic segments of Marcks-GFP transfected neurons; ADDL-/veh (n = 39), ADDL-/ReS19T (n=37), ADDL+/veh (n = 43) and ADDL+/ReS19T (n = 50). *: $p < 0.5$, ***: $p < 0.01$, ANOVA with pairwise comparisons of means (Tukey). Scale bar: 5 μm. (D) ADDL-induced cell death in neurons exposed to indicated treatments **: $p < 0.01$, t-test from 3 replicates. Error bars indicate 95% CI. (E) 3-hybrid

screen approach to identify ReS19T-interacting proteins. (F) *in-cellulo* interaction of MFC (ReS19T-929 linked to methotrexate) with different septin isoforms (n = 3, error bars: SD). Inset shows phylogenetic analysis of septin isoforms probed in 3-hydrid assay. (G-J) FIDA binding isotherms of ReS19T-127 to purified SEPT6, 7 and 2. (K-L) siRNA-mediated knockdown of SEPT6 attenuates ReS19T-127 effect on toxicity (K) and $[Ca^{2+}]_{cyto}$ (L) in ATRA-treated tau(P301L)-expressing BE(2)-M17 cells. See also corresponding Figs. S1-S3.

Identification and validation of septin 6 as a ReS19T target

To identify putative ReS19T targets, we carried out a three-hybrid screen in mammalian cells (*23*). We used as a prey a genome-wide collection of human open reading frames (ORFs) fused to truncated gp130 and as a bait ReS19T linked to methotrexate (MFC). Interaction of MFC with a prey turns on leptin-dependent STAT3 signaling and induces a STAT3-responsive reporter gene (Fig. 1E). Only three cDNAs elicited at least a two-fold induction of the reporter in presence of MFC compared to untreated cells (Fig. S2A). Among these three candidates, septin 6 (SEPT6) reproducibly evoked the strongest response (Fig. S2A). Re-screening of all septin isoforms present in the ORFeome collection confirmed binding of MFC to SEPT6 and revealed a weaker interaction with SEPT11, while none of the other septin isoforms tested interacted with MFC (Figs. 1F and S2B-D). A phylogenetic analysis of these septin isoforms showed that MFC interacts with the two most closely related SEPT6 family members (SEPT6 and SEPT11) and shows no detectable binding to the more distant SEPT2 and SEPT3 classes (Fig 1F). SEPT6 is a GTP-binding protein that assembles into filaments at the cell cortex together with SEPT2 and SEPT7 family members (*24*, *25*). Septins regulate microtubule dynamics (*26*) and are found, together with hyperphosphorylated tau, in neurofibrillary tangles of AD brains (*27*), pointing to a possible connection between tau and the septin cytoskeleton.

Next, we examined binding of ReS19T to purified septin isoforms (Fig. S3G) using flow-induced dispersion analysis (FIDA), a label- and immobilization-free technology that quantifies biomolecular interactions based on changes in size and diffusion (*28*). In these experiments, septin isoforms were maintained in high salt to prevent oligomerization. ReS19T induced a dose-dependent increase in SEPT6 hydrodynamic radius, which, when fitted to a binding isotherm equation, revealed a dissociation constant (K_d) of 1.5 nM (Figs. 1G and S3A). Measuring K_d based on binding-related (fluorescence) intensity change (BRIC) led to a comparable value (1.6 nM, Figs. 1H and S3D). No compound-induced changes in hydrodynamic radius were detected for SEPT7 and SEPT2 (Fig. S3B,C), although binding isotherms associated with higher dissociation constants were observed by BRIC for both isoforms (Figs. 1I,J and S3E,F). These cell-free binding studies demonstrate direct and high affinity binding of ReS19T to SEPT6 with a possible impact on the target conformation. They also provide evidence for weaker binding of the compound to SEPT7 and SEPT2.

RNAi-mediated silencing of SEPT6 attenuates modulation by ReS19T of both toxicity and $[Ca^{2+}]_{cyto}$ (Fig. 1K,L) confirming that the target is required for the observed pharmacodynamic effects. Silencing is not complete (Fig. S2E), hence compound action through residual SEPT6, or other septin isoforms is to be anticipated. SEPT6 knockdown resulted in elevated toxicity and $[Ca^{2+}]_{cyto}$ at ineffective compound concentrations (Fig. 1K,L) suggesting an inhibitory function of the target on $[Ca^{2+}]_{cyto.}$

ReS19T targets store-operated calcium entry

Septins have been identified as central regulators of store-operated calcium entry (SOCE) (*29*, *30*) – a form of calcium influx activated by calcium depletion from the ER. To examine the impact of tau on SOCE at the single-cell level, we transfected neuroblastoma cells with tauP301L-T2A-mRuby, tau-T2A-mRuby or mRuby DNA plasmids (Fig. S4A) and imaged SOCE by calcium addback following store depletion. tauP301L elicited a marked increase in basal $[Ca^{2+}]_{cyto}$ (before store depletion) and SOCE amplitude as compared to wt tau or the mRuby control (Figs. 1A and S4A-D). Selecting cells with increasing levels of tau expression (by gating mRuby intensity) revealed a corresponding increase in SOCE amplitude and $[Ca^{2+}]_{cyto}$ for both mutant and wt tau, although SOCE remained significantly larger in tauP301L-expressing cells (Fig. S4A,B). As expected, SOCE responses in cells expressing mRuby alone were not influenced by mRuby expression levels (Fig. S4B).

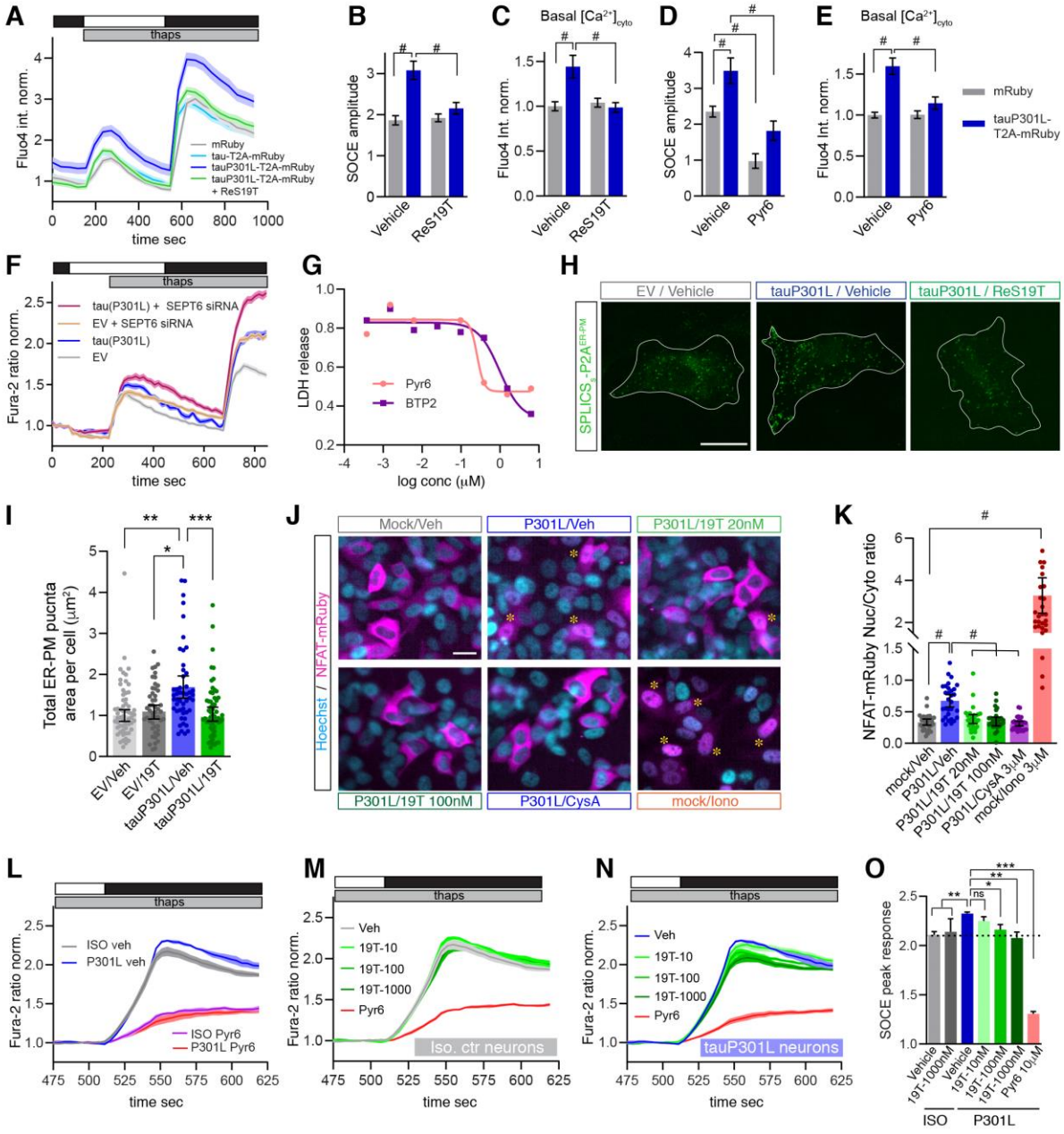

Fig. 2 ReS19T specifically targets a tau-dependent pathological form of SOCE. (A-C) SOCE measured by calcium addback in individual Fluo4-loaded BE(2)-M17 cells transfected with the indicated constructs and exposed to vehicle (DMSO) or ReS19T-127 200 nM (24 hrs). (A) Fluo4 traces are normalized to the control mRuby/vehicle condition. Extracellular calcium concentrations (black: 2 mM, white: 0 mM) and thapsigargin addition are indicated on top of time series. (B,C) Average SOCE amplitude (B) and basal $[Ca^{2+}]_{cyto}$ (C) derived from time series shown in A. (D,E) Independent calcium addback experiment showing average effect of Pyr6 10 μM (1 hr) on SOCE amplitude and basal $[Ca^{2+}]_{cyto}$ in mRuby- or tauP301L-T2A-mRuby-expressing cells. (A-E) More than 500 cells were analyzed for each condition. (F) SOCE measured in Fura-2 loaded BE(2)-M17 cells stably expressing tauP301L or EV and transfected with scrambled and SEPT6-targeting siRNAs. Shown are average calcium traces obtained from 24 replicate wells for each condition. (G) Dose-dependent inhibition of LDH release in tauP301L stably expressing and ATRA-treated cells by the SOCC inhibitors Pyr6 and BTP2. (H,I) Imaging and quantification of ER-PM contact sites in control and tauP301L cells treated with vehicle or ReS19T-127 (24hrs, 100nM). Scale bar: 10 μm. (J,K) NFAT activity measured by nuclear translocation of mRuby-NFAT3 in control or tauP301L-T2A-mRuby cells exposed to ReS19T-127 (48 hrs), cyclosporin A (3 μM, 1 hr) or ionomycin (10 μM, 1 hr). (J) Confocal images showing mRuby-NFAT localization in response to indicated treatments. Scale bar: 20 μm. (K) mRuby-NFAT nucleus to cytoplasm intensity ratio measured for indicated treatments. n = 30 cells for each condition. (L-O) SOCE in patient-derived glutamatergic neurons (tauP301L) and isogenic controls cultured for 90 days in vitro. Mean calcium traces showing $[Ca^{2+}]_{cyto}$ increase after calcium addback in store-depleted iPSC-derived neurons for the indicated genotype/treatment (3 replicate wells for each condition). (O) Quantification of peak SOCE responses in control and tau(P301L) neurons treated with increasing concentrations of ReS10T-127 for 24 hrs or Pyr6 (10 μM). (Shaded) error bars represent 95% CI. *: $p < 0.05$, **: $p < 0.01$, ***: $p < 0.001$ and #: $p < 0.0001$; One way ANOVA with multiple pairwise comparison of means (Tuckey test). See corresponding Fig. S4.

Exposure to 200 nM ReS19T was sufficient to bring down SOCE amplitude (Fig. 2A,B) and basal $[Ca^{2+}]_{cyto}$ (Fig. 2A,C) to control levels in tauP301L-T2A-mRuby cells. The compound lowered both calcium readouts in a dose-dependent manner (Fig. S4D,E). In marked contrast, ReS19T left SOCE amplitude (Fig. 2B) and basal $[Ca^{2+}]_{cyto}$ (Fig. 2C) unchanged in mRuby cells. Selective targeting of tau-induced SOCE by ReS19T was not observed with the Store-Operated Calcium Channel (SOCC) inhibitor Pyr6, which disrupted SOCE equally well in both tauP301L-T2A-mRuby and mRuby cells (Figs. 2D and S4F). Pyr6 also decreased basal $[Ca^{2+}]_{cyto}$ in tauP301L cells (Figs. 2E and S4F) confirming that aberrant SOCC activation is responsible for steady-state elevation of cytoplasmic calcium levels in the pathological state. Pyr6, however, had no effect on basal $[Ca^{2+}]_{cyto}$ in control cells (an hour after treatment) further implying that SOCE is far less active at steady state (in the absence of store depletion) unless tauP301L is expressed (Fig. 2E). Notably, mutant tau can stimulate SOCE in store-replete cells since ER calcium stores (and their release) are unaffected by tauP301L expression (Fig. 2A). Thus, the tauopathy-causing P301L mutation triggers a form of constitutive, store-independent but SOCC-mediated calcium entry which is not encountered in normal cells and specifically blocked by ReS19T.

We then probed the function of SEPT6 in regulating SOCE. RNAi-mediated knockdown of SEPT6 (Fig. S2E) resulted in a marked increase in SOCE, similar to that caused by tauP301L (Fig. 2F), pointing to an inhibitory effect of the ReS19T target on SOC channels, and providing a mechanism for elevated steady-state $[Ca^{2+}]_{cyto}$ in SEPT6-silenced cells (Fig. 1L). Combined perturbations further potentiated calcium entry in an additive manner (Fig. 2F).

To determine whether deranged SOCE and ensuing $[Ca^{2+}]_{cyto}$ overload mediate toxicity in our tauP301L cell model, we manipulated SOC channel activity both pharmacologically and genetically. Two inhibitors of SOC channels, Pyr6 and BTP2, attenuated cell death (Fig. 2G) with IC50s near the potencies of the drugs for Orai channel inactivation (*31*). Similarly, siRNA-mediated knockdown of stromal interaction molecule 1 (Stim1) – an essential component of the SOCE machinery (*29*, *30*) – suppressed toxicity and occluded compound effect (Fig. S5A-D). Finally, toxicity could also be alleviated (Fig. S5E) by pharmacological stabilization of septin

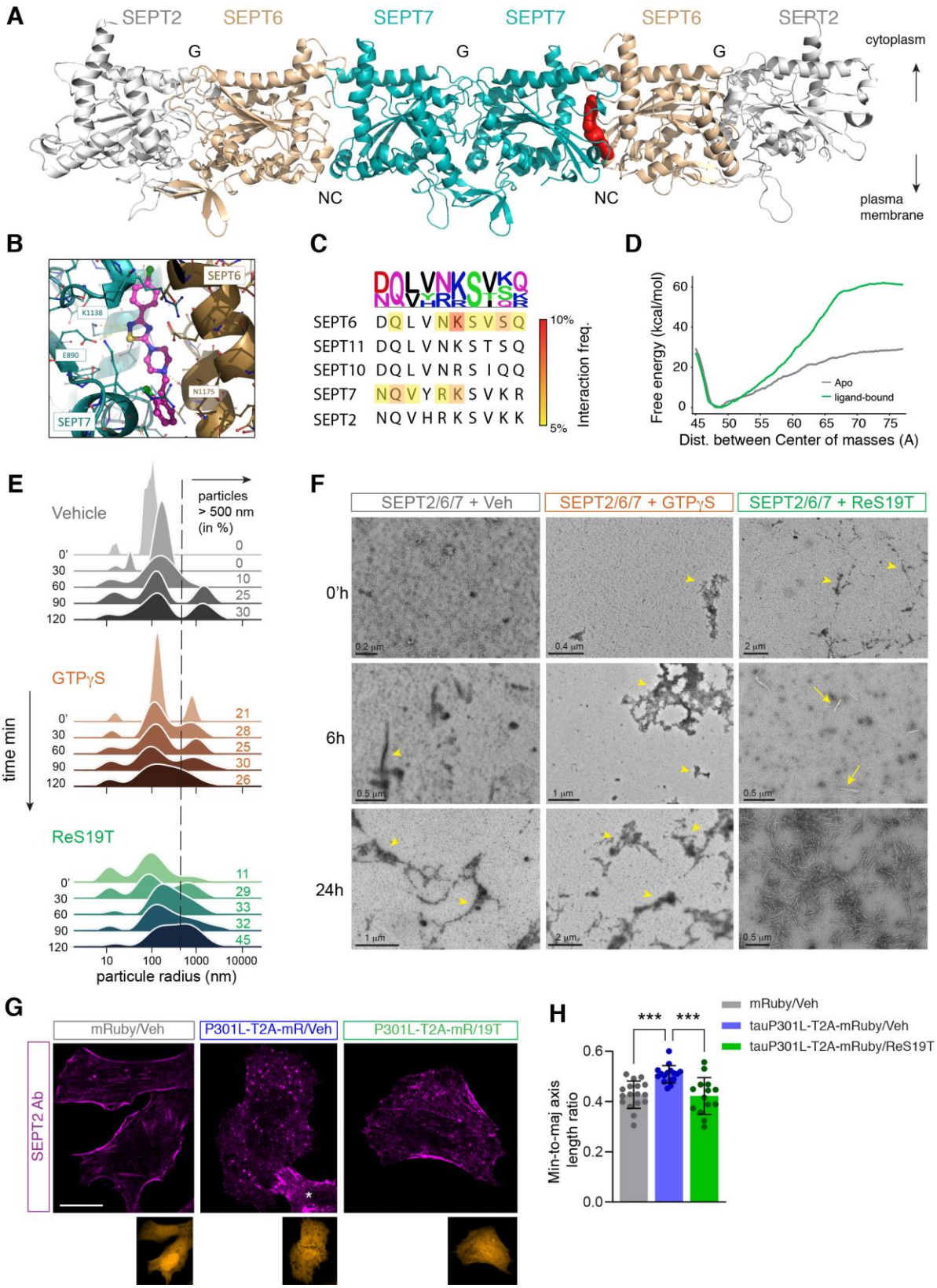
A
SEPT2
SEPT6
SEPT7
SEPT7
SEPT6
SEPT2
G
G
G
NC
NC
cytoplasm
plasma membrane
B
SEPT6
K1138
E890
N1175
SEPT7
C
SEPT6 DQLVNKSVSQ
SEPT11 DQLVNKSTSQ
SEPT10 DQLVNRSIQQ
SEPT7 NQVYRKSVKR
SEPT2 NQVHRKSVKK
10%
5%
Interaction freq.
D
Free energy (kcal/mol)
Apo
ligand-bound
Dist. between Center of masses (A)
E
Vehicle
particles > 500 nm (in %)
GTPγS
ReS19T
time min
particule radius (nm)
F
SEPT2/6/7 + Veh
SEPT2/6/7 + GTPγS
SEPT2/6/7 + ReS19T
0'h
6h
24h
G
mRuby/Veh
P301L-T2A-mR/Veh
P301L-T2A-mR/19T
SEPT2 Ab
H
mRuby/Veh
tauP301L-T2A-mRuby/Veh
tauP301L-T2A-mRuby/ReS19T
Min-to-maj axis length ratio

Fig. 3 ReS19T influences dynamics of Septin filament assembly. (A-D) LiGaMD simulations of ReS19T-127 interaction with the SEPT2/6/7 hexamer. (A) LiGaMD identifies a high-affinity binding pocket at the NC interface between SEPT6 and SEPT7. ReS19T-127 is shown in red. (B) Blow up of the SEPT6/7 interface with amino acids predicted to interact with ReS19T. Hydrogen bonds formed by the compound with surrounding amino acids are shown in yellow. Amino acids are labeled according to their position in the SEPT2/6/7 hexamer. (C) Alignment showing main cluster of amino acids in SEPT6 and SEPT7 interacting with ReS19T. Heatmap indicates frequency of interaction. Amino acid conservation and type is shown on top using sequence logo. (D) Umbrella sampling calculations of the SEPT6/7 heterodimer showing binding free energy with and without bound ligand. (E,F) Cell-free assembly of SEPT2/6/7 filaments. (E) Dynamic light scattering measurements performed at different time points after mixing of purified SEPT2, 6 and 7 (500 nM final protein concentration), in presence of vehicle (DMSO), GTPγS (100 μM) or ReS19T-127 (1 μM). 0' indicates first measurement immediately after component mixing. Distribution of particle size (y axis) are normalized across treatment and time points. (F) TEM images of SEPT2/6/7 polymerization performed in conditions identical to (E) and captured at three time points after component mixing. Arrows heads point to typical polymerized structures. Arrows point to highly ordered filaments only observed after ReS19T-127 treatment. (G,H) SEPT2 immunostaining in BE(2)-M17 cells transfected with mRuby or tauP301L-T2A-mRuby and treated for 24hrs with ReS19T-127 (100 nM) or vehicle. (G) mRuby channel is shown below. The Asterisk indicates a non-transfected cell. Scale bar: 10 μm. (H) Quantification of SEPT2 circular vs filamentous structures by measuring the average minor to major axis length ratio for all SEPT2 objects segmented in individual cells. $p < 0.0001$, One way ANOVA with pairwise comparisons of means (Tukey). See also corresponding Fig. S6.

assembly with the small molecule forchlorfenuron (*32*), a perturbation reported to impair SOCE (*29*).

SOCCs are activated by the ER-resident Stim proteins at contact sites between the ER and the plasma membrane (PM). We thus examined whether tau regulates the formation of ER-PM contact sites using the $SPLICS_{short}$-$P2A^{ER-PM}$ probe, which specifically labels these membrane appositions (*33*). tauP301L augments the interaction of the ER with the PM and the increased contact area between these two membrane systems is lowered by ReS19T (Fig. 2H,I) in agreement with the inhibitory effect of the compound on tau-induced SOCE.

To assess the impact of ReS19T on calcium effector pathways, we focused on the calcium/calmodulin-dependent phosphatase calcineurin (CaN), which activates the transcription factor NFAT. Aberrant CaN/NFAT activity has been implicated in Aβ (*34*) and tau (*35*) pathology. tauP301L induces translocation of NFAT to the nucleus (in the absence of store depletion), and tau-mediated activation of this transcription factor is fully inhibited by 100 nM ReS19T, or the CaN inhibitor cyclosporin A (Fig. 2J,K) indicating that calcium-dependent signaling is normalized by the lead compound.

To examine SOCE in a more clinically relevant disease model, we turned to patient iPSC-derived glutamatergic neurons. Neurons carrying the tauP301L mutation showed a slight but significant increase in store-operated calcium influx compared to their isogenic controls (Figs. 2L,O and S4H,I) confirming enhanced SOC channel activity under conditions of tau pathology. ReS19T decreased SOCE in tau(P301L) neurons in a dose-dependent manner (Fig. 2N,O) but had no detectable effect on SOCE in control neurons (Fig. 2M,O). Maximal SOCE inhibition by ReS19T reached levels observed in untreated isogenic neurons, while blockade of SOC channels with Pyr6 resulted in a pronounced inhibition of calcium entry in both control and tauP301L neurons (Fig. 2L-O).

Septins have recently been shown to regulate the number of ER-PM contact sites (*29*, *30*), pinpointing a possible mechanism of action for ReS19T. To test the influence of ReS19T on the septin cytoskeleton, we first explored the space of potential binding pockets in the palindromic SEPT2/6/7 hexamer (Fig. 3A), which forms the minimal core unit for filament polymerization. To this end, we used Ligand Gaussian Accelerated Molecular Dynamics (LiGaMD), a computational

method particularly suited to sample the entire conformational space of a ligand around a protein of interest (*36*). A recent CryoEM structure of the SEPT2/6/7 hexamer (*37*) refined with AlphaFold (*38*) was used for these simulations. Because septins are guanosine nucleotide-binding proteins, we considered eight simulation systems each differing in the number of GDP or GTP molecules (Fig S6A). ReS19T binding hotspots were identified at the SEPT6/7 interface in seven systems (Fig. S6A). In the nucleotide-free system, ReS19T binds near the SEPT7 GDP-binding pocket with the weakest affinity (Fig. S6A). In septin oligomers, subunits present alternating NC (N- and C-termini) and G (GTP-binding) interfaces (Fig. 3A). The SEPT6/7 interface is of the NC kind, consistent with minimal influence of GDP/GTP occupancy on ReS19T binding.

Fig. 3A shows the simulation outcome with the most energetically favorable ReS19T binding pose. ReS19T lies deep in the SEPT6/7 NC interface (Fig. 3A,B) and makes direct contact with several amino acids located on both SEPT6 and SEPT7 (Fig. 3B,C). The compound also makes hydrogen bonds with the backbone oxygen of asparagine 1175 on SEPT6 and possibly with glutamate 890 and/or lysine 1138 on SEPT7 depending on the protonation state of its thiadiazole ring (Fig. 3B). Extensive contact of the compound along the SEPT6/7 interface suggests a possible impact on SEPT6/7 dimer conformation/stability. To address this computationally, we measured binding free energy between septin 6 and 7 in the presence or absence of ReS19T and in response to a wide range of pulling forces until complete disruption of the dimer. These umbrella sampling calculations revealed an endpoint difference of 30 kcal/mol between ligand-bound and ligand-free states (Fig. 3D) indicating that disruption of the ligand-bound system is energetically more costly and suggesting therefore stabilization of the SEPT6/7 dimer by ReS19T.

Since ReS19T binds to purified SEPT6 alone (Fig. 1G,H), we employed LiGaMD to simulate binding of the compound to the SEPT6 homodimer which is the preferred state of purified septins in non-polymerizing conditions. Modeling of the SEPT6 homodimer by AlphaFold predicted an NC interface (Fig. S6B,C) like the one observed at the SEPT6/7 interface in the septin hexamer. LiGaMD identified a ReS19T binding hotspot in the cavity created by the NC interface in the SEPT6 homodimer (Fig. 6D).

ReS19T influences dynamics of septin filament assembly

To experimentally interrogate the effect of ReS19T on septin polymerization, we mixed purified septin 2, 6 and 7 in conditions that favor filament assembly and monitored polymerization at different time points by dynamic light scattering (DLS) and transmission electron microscopy (TEM). A clear shift towards higher particle sizes (above 500 nm) was detected by DLS 90 min after component mixing (Fig. 3E). Addition of GTPγS – a non-hydrolysable form of GTP that speeds up septin assembly – accelerated the formation of larger particles with an effect noticeable immediately after component mixing (Fig. 3E). Likewise, ReS19T shifted the distribution of particles towards larger sizes with kinetics comparable to GTPγS. Consistent with these DLS measurements, TEM images showed that both GTPγS and ReS19T induced the formation of polymerized structures shortly after component mixing (Fig. 3F). No or few such structures were detectable in the vehicle condition at early time points (Fig. 3F). At 6h post-mixing, highly ordered filaments appeared in the ReS19T-treated samples, the number of which dramatically increased in the following 18h (Fig. 3F). Although micrometer-long polymers were also observed in vehicle and GTPγS conditions 24h post-mixing, their structure significantly differed from the linear

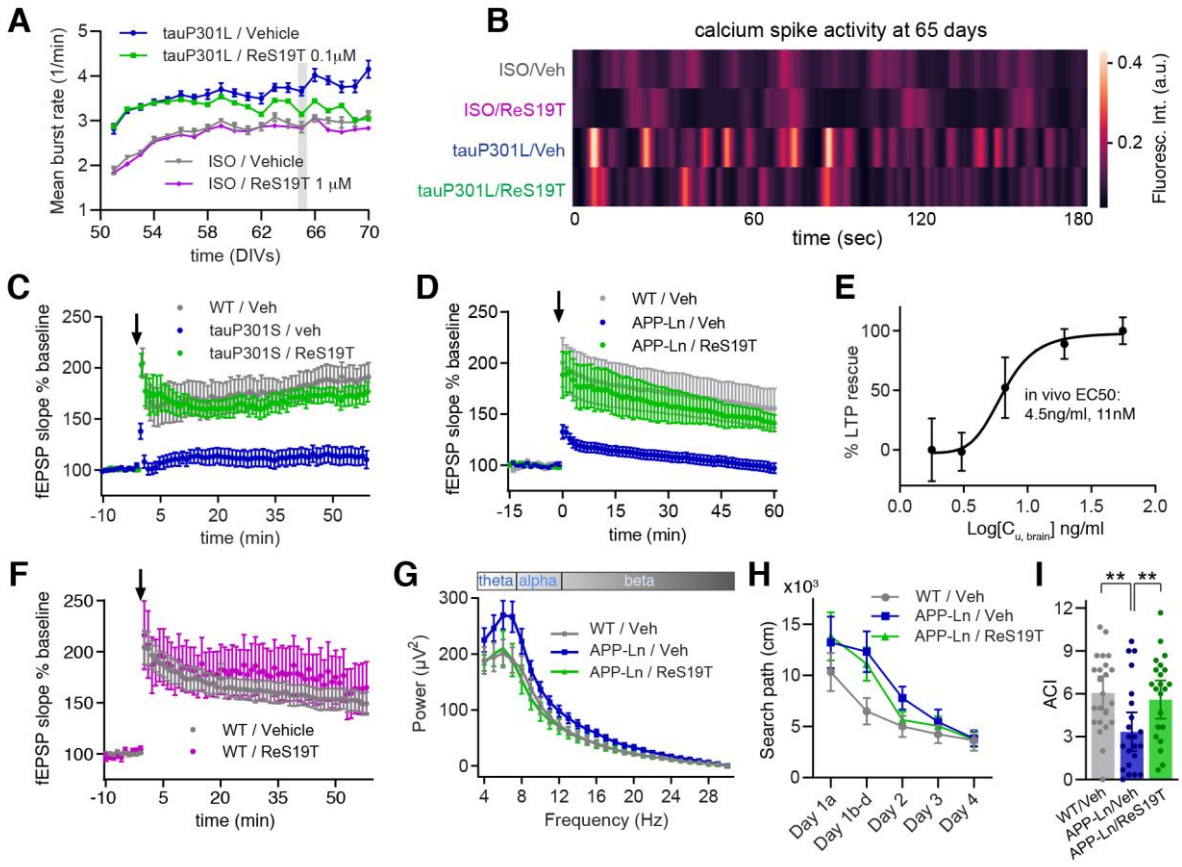

Fig. 4 Rapid restoration of synaptic network and cognitive functions by ReS19T in AD preclinical models. (A) Calcium spike activity reflecting spontaneous firing of patient-derived tau(P301L) neurons and their isogenic controls exposed to vehicle or 100 nM ReS19T-127. Mean frequency of calcium bursts was measured during 3 min over a period of 20 days, from DIV 50 to 70. (B) Calcium spike activity measured 15 days after the first recording and corresponding to time point highlighted in grey in (A). (C) CA1 L-LTP in WT/Veh (n=5), hAPP-Ln/Veh (n=6) and hAPP-Ln/ReS19T-127 (n=6) mice (7 months of age) administered with vehicle or ReS19T-127 (20mg/kg/day) for 7 days. Arrow: tetanus L-LTP inducing stimulus. ***: $p < 0.001$, pairwise comparison of vehicle vs ReS19T-127 treated hAPP-Ln animals (Tuckey's test). (D) Exposure-dependent rescue of L-LTP in hAPP-Ln mice. $C_{u,brain}$: average free brain concentration of ReS19T-127 calculated from *in vivo* pharmacokinetic profile of the compound. (E) CA1 L-LTP in WT and htau(P301S) mice (3.5 months of age, n = 8 for each group) administered with vehicle or ReS19T-127 (20mg/kg/day) for 2 months. ***: $p < 0.001$, pairwise comparison of vehicle vs ReS19T-127 treated htau(P301S) animals (Tuckey's test). (F) L-LTP in WT animals (3.5 months of age) administered with vehicle (n = 11) or ReS19T-127 (n = 6) at 20mg/kg/day for 7 days. (G) Power analysis of EEG recordings (parietal lobe) in awake WT/Veh (n=6), hAPP-Ln/Veh (n=4) and hAPP-Ln/ReS19T-127 (n=4) mice, 8 months of age, administered with vehicle of ReS19T-127 for 14 days. **** $p <$ (treatment effect) < 0.0001. Two-way ANOVA with repeated measures. Error bars indicate SEM. (G,H) Morris water maze. Spatial learning (H) and probe trial (I) in WT/Veh (n=23), hAPP-Ln/Veh (n=23) and hAPP-Ln/ReS19T-123 (n=23) mice, 8 months of age, administered with vehicle or ReS19T-123 (20mg/kg/day) for 11 weeks. Error bars indicate SEM. ****: $p < 0.0001$, Two-way ANOVA with repeated measures (H). **: $p < 0.01$, t-test (I).

pattern of polymerization generated by ReS19T, suggesting distinct mechanisms of action. In support of this view, ReS19T is predicted to bind and stabilize the SEPT6/7 NC interface, while GTP (and GTPγS) interacts with G interfaces in the polymer.

To assess whether septin filaments are influenced by tau and ReS19T within cells, we monitored the endogenous state of septin polymerization. Because SEPT6 antibodies failed to label distinct cytoskeletal structures, we used instead a SEPT2 antibody which stains filaments that co-localize

with exogenous GFP-SEPT6 (Fig. S7). In control conditions, SEPT2 typically localizes to filaments at the cell cortex, but these undergo major remodeling to circular doughnut-like structures in response to tauP301L expression (Figs. 3G). Strikingly, treatment with ReS19T (100 nM) restores the fibrillar organization of SEPT2 near the plasma membrane (Fig. 3G,H).

Collectively, these experiments support the following sequence of events: tauP301L destabilizes the cortical septin cytoskeleton, resulting in increased ER-PM contact area and constitutive activation of SOCCs. By restoring filament assembly at the plasma membrane, ReS19T limits ER-PM contacts and keeps activity of SOCCs in check.

Modulation of SEPT6 by ReS19T restores network function in patient-derived iPSC-neurons and AD mouse models

$[Ca^{2+}]_{cyto}$ overload has been associated with hyperexcitability and synaptic dysfunction in AD. To assess whether patient-derived excitatory neurons are hyperexcitable, we compared spontaneous firing frequency of glutaminergic tauP301L neurons and their isogenic controls by longitudinal measurements of calcium spike activity over the course of 20 days. The mean burst rate was markedly increased in tauP301L neurons at all time points investigated, and this hyperexcitability phenotype was progressively and fully rescued by ReS19T (Fig. 4A,B).

The effect of ReS19T on synaptic plasticity was next examined in transgenic mice expressing either human tauP301S, a mutation causing frontotemporal dementia (*39*), or the APP London mutant carrying the familial AD mutation V717I. Both models of neurodegeneration show severe deficits in long-term potentiation (LTP) in the CA1 region of the hippocampus (Fig. 4C,D), a form of activity- and calcium-dependent increase in synaptic efficacy associated with the acquisition of new memories. Oral administration of ReS19T restored LTP in tauP301S and APP-Ln mice to levels undistinguishable from WT animals (Fig. 4C, D). Pharmacokinetics studies in mice enabled us to establish the exposure-response relationship and revealed an effective dose (ED50) of 6 mg/kg, corresponding to an average unbound concentration in brain of 11 nM (Fig. 4E), which agrees with the potency of the compound *in vitro* (Fig. 1A). ReS19T had no significant effect on LTP in WT animals (Fig. 4F), further supporting a disease-specific mechanism of action.

Rapid modulation of neuronal excitability and synaptic plasticity by ReS19T prompted us to test the influence of the compound on brain oscillatory activity. In AD patients electroencephalography (EEG) recordings indicate increased power in low-frequency theta rhythms, which correlates with poor cognitive performance and is increasingly recognized as a potential biomarker (*40*, *41*). Likewise, a higher magnitude of low-frequency bands is observed in awake APP-Ln mice (Fig. 4G). Administration of ReS19T for two weeks normalized power spectral density to control levels (Fig. 4G), demonstrating broad impact of our lead compound on network function.

We then tested the ability of ReS19T to rescue spatial memory deficits in APP-Ln mice using the Morris water maze. These mice showed an initial delay in spatial learning, but by the end of the fourth training day, they located the hidden escape platform with the same efficiency as their non-transgenic counterparts (Fig. 4H). Eleven weeks treatment of APP-Ln mice with ReS19T had no significant effect on this mild learning delay (Fig. 4H). In the probe trial, APP-Ln mice displayed a marked deficit in spatial memory, which was fully rescued by treatment with ReS19T (Fig. 4I), suggesting restoration of neural circuits that underlie retrieval of spatial memories.

ReS19T mitigates development of AD pathology

Apart from mediating degeneration of neurons, aberrant calcium signaling is also thought to promote development of AD pathology (*42–44*). Therefore, we hypothesized that restraining calcium influx in diseased neurons by ReS19T should mitigate AD pathology in AD mouse models. Treatment of bigenic hAPP-Ln:PS1(A246E) with ReS19T for three months resulted in a 55-60% reduction of Aβ plaque build-up in the neocortex (Fig. 6A,B) and subiculum (Fig. 5A,C), a structure that connects the entorhinal cortex to the hippocampus – both brain regions are heavily affected in AD. In the same mutant mice, the compound also reduced microglial inflammation associated with AD pathology (Fig. 5D).

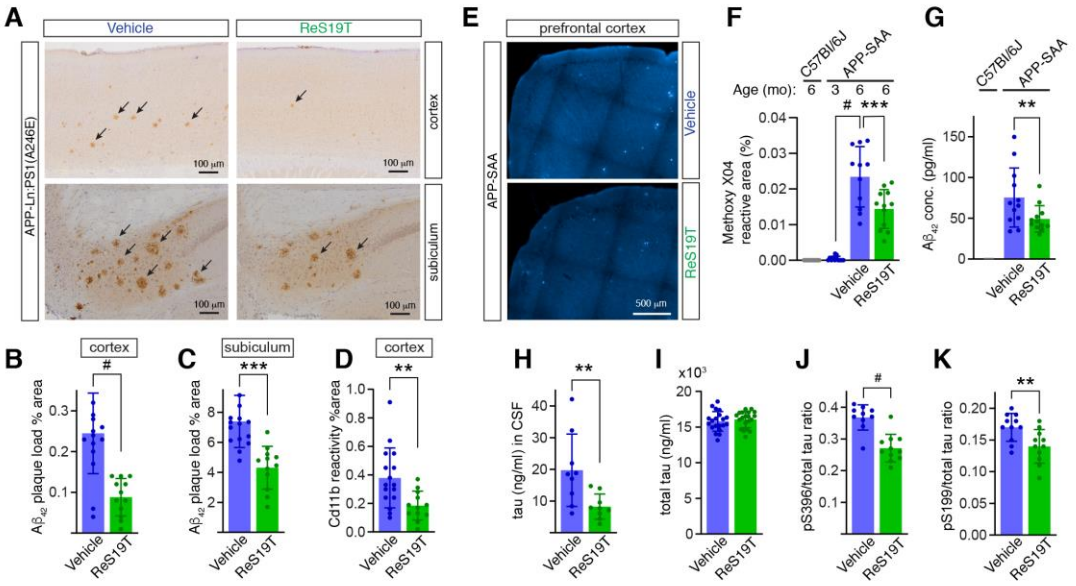

Fig. 5. ReS19T attenuates AD pathology. (A-D) hAPP-Ln:PS1(A246E) mice (7 months old) after 3 months of vehicle (n = 16) or ReS19T-127 (n = 14) oral dosing at 20 mg/kg/day. (A-C) Amyloid plaque immunoreactivity in cortex (A,B) and subiculum (A,C). (D) CD11b immunoreactivity in cortex. (E-G) Dense core staining of Aβ plaques in prefrontal cortex (E,F) and measurements of $A\beta_{42}$ concentration in brain extracts (G) of APP-SAA mice and C57B/6J controls orally dosed with vehicle or ReS19T-129 (25mg/kg/day) for 2 months. n = 12 for each group. (H-K) 5 months old tauP301S mice treated for 3 months with vehicle or ReS129T-123 at 20mg/kg/day. (H) Tau levels in CSF measured by ELISA (n = 9 for each group). Pan-Tau (I), pS396-tau (J) and pS199-tau (K) measured by ELISA in cortical extracts (n = 10 for each group). **: $p < 0.01$, **: $p < 0.001$, #: $p < 0.0001$ Error bars: SDM.

ReS19T also reduced Aβ plaque load (Fig. 5E,F) and $A\beta_{42}$ production (Fig. G) in the prefrontal cortex of APP-SAA mice, a knock-in AD model recently developed by Denali that exhibits age-dependent accumulation of amyloid plaques (*45*). Finally, treatment of tauP301S mice with ReS19T significantly lowered levels of tau in cerebrospinal fluid (CSF) (Fig. 5H) – a clinical AD biomarker, in line with calcium-dependent tau secretion (*46*), and decreased tau phosphorylation in cortical brain extracts of these mice (Fig. 5I-K). Thus, ReS19T attenuates the main pathological features of AD.

Discussion

Prolonged elevation of cytosolic calcium is hypothesized to play a central role in AD (*9*). On the one hand, aberrant $[Ca^{2+}]_{cyto}$ drives key elements of AD pathobiology including Aβ aggregation, tau phosphorylation, neuro-inflammation and mitochondrial dysfunction. On the other hand, calcium overload mediates some of the neurotoxic effects of Aβ and tau species, both in early

(disruption of synaptic plasticity) and late (synapse and neuronal loss) stages of disease. Such a central bidirectional role of calcium in AD pathogenesis predicts that interventions restoring calcium homeostasis should exert fast and broad-acting therapeutic effects (*14*). Here we reveal the therapeutic benefits of a novel class of small molecules (ReS19T) that target calcium dysregulation induced by pathological tau, providing further support for a key role of aberrant $[Ca^{2+}]_{cyto}$ in driving neurodegeneration.

A 7-day ReS19T treatment of APP-Ln mice, an APP AD model that exhibits early tau hyperphosphorylation (ref), is sufficient for full restoration of hippocampal LTP, indicating fast relief of Aβ and tau-driven toxicity on the underlying neural circuits. This therapeutic effect is consistent with fast-acting decrease in $[Ca^{2+}]_{cyto}$ by ReS19T and down-regulation of CaN activity, a calcium-activated phosphatase centrally implicated in synaptic depression, memory erasure and Aβ-induced synapse disruption (*49*, *50*). ReS19T also mitigates amyloid plaque burden in two distinct AD mouse models (APP-Ln and APP-SAA), decreases the production of pathological Aβ and tau, and reduces neuroinflammation indicating activity both upstream and downstream of Aβ/tau. The effects of the compound can thus be attributed to rapid interruption of a self-reinforcing cycle of pathophysiological events fueled by elevated cytosolic calcium.

Our findings demonstrated that aberrant calcium entry is an integral component of tau pathology, in agreement with a recent study that identified genes associated with altered calcium homeostasis as primary modifiers of tau-induced toxicity (*47*). Accumulating evidence points to synergistic pathological interaction and reciprocal influence of Aβ and tau in AD (*48*). While the impact of Aβ on the initiation of tau pathology is undisputed – tau is hyperphosphorylated in many APP models (including the ones used here), and in response to challenge with soluble Aβ oligomers – tau has also been shown to enhance and, in some cases, mediate aspects of Aβ pathology (ref). In light of these observations, we surmise that the inhibitory effect of ReS19T on Aβ pathology (Aβ plaques and $Aβ_{42}$ levels) is due, at least in part, to its normalizing activity on tau-induced calcium dysregulation.

ReS19T targets a form of pathological activation of SOCE mediated by a tau mutation (P301L) causing FTD. Because this mutation is linked to tau hyperphosphorylation and aggregation (hallmarks of all tauopathies, including AD) we propose that similar disease and compound mechanisms are at play in AD.

We provide evidence that tau-induced SOCC activation and compound activity are both linked to the septin cytoskeleton. In non-pathological conditions, septin filament assembly at the cell cortex restrains SOCE and inhibits constitutive (store-independent) activation of SOCCs. In support of this "gate keeper" function, silencing of SEPT6 (this study) or SEPT7 (*30*, *51*, *52*) results in unimpeded SOCE activity. Knockdown of SEPT2 family members (SEPT2, SEPT4 and SEPT5), in contrast, has been reported to suppress SOCE (*29*), highlighting complex modulatory roles of septin isoforms in SOCC regulation. In conditions of tau pathology, fibrillar organization of the septin cytoskeleton at the plasma membrane is disrupted and this is associated with an increase in ER-PM contact sites, thus providing a mechanism for uncontrolled activation of SOCCs. By restoring septin organization at the cell cortex in the disease state, ReS19T rehabilitates an important element of physiological SOCC regulation, which prevents spurious activation of the channel in store-replete conditions.

Together, these findings reveal a mechanism of action restricted to the pathological state where ReS19T operates on a form of deviant SOCC activation only found in conditions of tau pathology. Accordingly, the compound doesn't interfere with physiological (receptor-mediated) ER calcium

release and SOCE signaling (Fig. S5F), nor does it influence other calcium signaling systems involved in synaptic plasticity (LTP) in non-pathological conditions.

Perturbed expression and mislocalization of different septin isoforms have previously been associated with neurodegeneration. SEPT1, SEPT2 and SEPT4 are found in neurofibrillary tangles and dystrophic neurites in AD (*27*), while SEPT4 colocalizes with α-synuclein in Parkinson's disease Lewy bodies (*53*), and SEPT11 – a close homolog of SEPT6 – is enriched in insoluble fractions in frontotemporal lobar degeneration (*54*). We show here for the first time that pharmacological modulation of septin assembly results in broad neuroprotective effects in both cell- and animal models of AD suggesting a central role of septin filaments in AD pathogenesis.

In summary, this work highlights the therapeutic potential of calcium-lowering interventions in AD and other tauopathies. Whether therapeutic benefits observed in experimental models of AD will translate to patients awaits completion of ongoing clinical trials, but the observation that chronic treatment of organ-transplant patients with CaN inhibitors protects against AD and dementia (*55*), provides epidemiologic support for this therapeutic strategy.

Acknowledgments: We thank Kritika Sahni Ray, Marion Albasini and Henrik Jensen (Fidabio) for their expertise and guidance in all FIDA experiments. We are in debt to Prof. Bart de Strooper for his scientific advice. We thank Prof Patrick Verstreken and Prof Georg Halder for critical reading of the manuscript and the Bioimaging Core (VIB, Leuven) for training, technical support and access to the instrument park.

Funding: reMYND was funded by grants from the Flanders Innovation & Entrepreneurship (VLAIO) formerly known as Institute for the Promotion of Innovation by Science and Technology in Flanders (Project numbers 030383, 070157, 080394, 090494). The Switch lab was supported by the Flanders Institute of Biotechnology (VIB, grant no. C0401 to FR and JS); KU Leuven; the Fund for Scientific Research Flanders (FWO, Postdoctoral Fellowships 12P0919N and 12P0922N to NL); and Stichting Alzheimer Onderzoek / Fondation recherche Alzheimer (SAO-FRA 2022/0020 to NL. WA is supported by VIB, KU Leuven (C14/21/095 and SMINF KA/20/085), the FWO (G078117N, G056017N, G0C4220N and I001322N), SAO-FRA (#2020/030 and 2022/022) and the Alzheimer Association (AARF-22-968022 to XY).

Author contributions:
Conceptualization: GG, KP, TVD, MF
Methodology: KP, TVD, MD, NL, XW, NVD, IB, KC, SD, EC, AL, ML, SC, HD, OR, TV, MG, SV, LDR, SCl, YB, SL, JT, SHA, MV, MF, GG
Investigation: KP, TVD, SL, JT, MV, JW, SW, MF, GG
Funding acquisition: KDW, GG
Project administration: KP, TVD, LP, VV, ED, KDW, MF, GG
Supervision: GG, KP, TVD, VV, LP, MF
Writing – original draft: MF, GG
Writing – review and editing: MF, GG, HZ, JLC

Competing interests:

HZ has served at scientific advisory boards and/or as a consultant for Abbvie, Alector, Annexon, Apellis, Artery Therapeutics, AZTherapies, CogRx, Denali, Eisai, Nervgen, Novo Nordisk, Pinteon Therapeutics, Red Abbey Labs, reMYND, Passage Bio, Roche, Samumed, Siemens

Healthineers, Triplet Therapeutics, and Wave, has given lectures in symposia sponsored by Cellectricon, Fujirebio, Alzecure, Biogen, and Roche, and is a co-founder of Brain Biomarker Solutions in Gothenburg AB (BBS), which is a part of the GU Ventures Incubator Program (outside submitted work). JC has provided consultation to Acadia, Alkahest, AlphaCognition, AriBio, Biogen, Cassava, Cortexyme, Diadem, EIP Pharma, Eisai, GemVax, Genentech, Green Valley, Grifols, Janssen, Karuna, Lilly, Lundbeck, LSP, Merck, NervGen, Novo Nordisk, Oligomerix, Ono, Otsuka, PRODEO, Prothena, ReMYND, Resverlogix, Roche, Signant Health, Suven, and United Neuroscience pharmaceutical, assessment, and investment companies. JW and SW are co-founders and shareholders of reMYND. GG is consultant for reMYND and owns reMYND warrants and shares. MF owns reMYND warrants.

References

1. P. Scheltens *et al.*, Alzheimer's disease. *Lancet*. **397**, 1577–1590 (2021).
2. M. A. Leissring *et al.*, Capacitative calcium entry deficits and elevated luminal calcium content in mutant presenilin-1 knockin mice. *J. Cell Biol.* **149**, 793–798 (2000).
3. R. Etcheberrigaray *et al.*, Calcium responses in fibroblasts from asymptomatic members of Alzheimer's disease families. *Neurobiol. Dis.* **5**, 37–45 (1998).
4. Q. Guo *et al.*, Increased vulnerability of hippocampal neurons to excitotoxic necrosis in presenilin-1 mutant knock-in mice. *Nat. Med.* **5**, 101–106 (1999).
5. J. Larson, G. Lynch, D. Games, P. Seubert, Alterations in synaptic transmission and long-term potentiation in hippocampal slices from young and aged PDAPP mice. *Brain Res.* **840**, 23–35 (1999).
6. S. Chakroborty *et al.*, Early presynaptic and postsynaptic calcium signaling abnormalities mask underlying synaptic depression in presymptomatic Alzheimer's disease mice. *J. Neurosci.* **32**, 8341–8353 (2012).
7. S. Forner, D. Baglietto-Vargas, A. C. Martini, L. Trujillo-Estrada, F. M. LaFerla, Synaptic impairment in alzheimer's disease: A dysregulated symphony. *Trends Neurosci.* **40**, 347–357 (2017).
8. D. J. Selkoe, Alzheimer's disease is a synaptic failure. *Science*. **298**, 789–791 (2002).
9. M. J. Berridge, Calcium regulation of neural rhythms, memory and Alzheimer's disease. *J. Physiol. (Lond.)*. **592**, 281–293 (2014).
10. E. Popugaeva, D. Chernyuk, I. Bezprozvanny, Reversal of calcium dysregulation as potential approach for treating alzheimer's disease. *Curr Alzheimer Res*. **17**, 344–354 (2020).
11. H. Hsieh *et al.*, AMPAR removal underlies Abeta-induced synaptic depression and dendritic spine loss. *Neuron*. **52**, 831–843 (2006).
12. S. H. Zaman *et al.*, Enhanced synaptic potentiation in transgenic mice expressing presenilin 1 familial Alzheimer's disease mutation is normalized with a benzodiazepine. *Neurobiol. Dis.* **7**, 54–63 (2000).
13. S. Chakroborty, I. Goussakov, M. B. Miller, G. E. Stutzmann, Deviant ryanodine receptor-mediated calcium release resets synaptic homeostasis in presymptomatic 3xTg-AD mice. *J. Neurosci.* **29**, 9458–9470 (2009).
14. E. K. Webber, M. Fivaz, G. E. Stutzmann, G. Griffioen, Cytosolic calcium: Judge, jury and executioner of neurodegeneration in Alzheimer's disease and beyond. *Alzheimers Dement.* **19**, 3701–3717 (2023).
15. S. I. Mota, I. L. Ferreira, A. C. Rego, Dysfunctional synapse in Alzheimer's disease - A focus on NMDA receptors. *Neuropharmacology*. **76 Pt A**, 16–26 (2014).
16. T. S. Anekonda *et al.*, L-type voltage-gated calcium channel blockade with isradipine as a therapeutic strategy for Alzheimer's disease. *Neurobiol. Dis.* **41**, 62–70 (2011).
17. M. Calvo-Rodriguez *et al.*, Increased mitochondrial calcium levels associated with neuronal death in a mouse model of Alzheimer's disease. *Nat. Commun.* **11**, 2146 (2020).
18. K.-H. Cheung *et al.*, Mechanism of Ca2+ disruption in Alzheimer's disease by presenilin regulation of InsP3 receptor channel gating. *Neuron*. **58**, 871–883 (2008).
19. J. Ye *et al.*, Tau-induced upregulation of C/EBPβ-TRPC1-SOCE signaling aggravates tauopathies: A vicious cycle in Alzheimer neurodegeneration. *Aging Cell*. **19**, e13209 (2020).

20. Z. Sun *et al.*, SOCE-mediated NFAT1-NOX2-NLRP1 inflammasome involves in lipopolysaccharide-induced neuronal damage and Aβ generation. *Mol. Neurobiol.* **59**, 3183–3205 (2022).
21. M. Dumbacher *et al.*, Modifying Rap1-signalling by targeting Pde6δ is neuroprotective in models of Alzheimer's disease. *Mol. Neurodegener.* **13**, 50 (2018).
22. J. Götz, G. Halliday, R. M. Nisbet, Molecular pathogenesis of the tauopathies. *Annu. Rev. Pathol.* **14**, 239–261 (2019).
23. M. Caligiuri *et al.*, MASPIT: three-hybrid trap for quantitative proteome fingerprinting of small molecule-protein interactions in mammalian cells. *Chem. Biol.* **13**, 711–722 (2006).
24. A. A. Bridges, A. S. Gladfelter, Septin form and function at the cell cortex. *J. Biol. Chem.* **290**, 17173–17180 (2015).
25. S. Mostowy, P. Cossart, Septins: the fourth component of the cytoskeleton. *Nat. Rev. Mol. Cell Biol.* **13**, 183–194 (2012).
26. J. R. Bowen, D. Hwang, X. Bai, D. Roy, E. T. Spiliotis, Septin GTPases spatially guide microtubule organization and plus end dynamics in polarizing epithelia. *J. Cell Biol.* **194**, 187–197 (2011).
27. A. Kinoshita *et al.*, Identification of septins in neurofibrillary tangles in Alzheimer's disease. *Am. J. Pathol.* **153**, 1551–1560 (1998).
28. M. E. Pedersen, J. Østergaard, H. Jensen, Flow-Induced Dispersion Analysis (FIDA) for Protein Quantification and Characterization. *Methods Mol. Biol.* **1972**, 109–123 (2019).
29. S. Sharma *et al.*, An siRNA screen for NFAT activation identifies septins as coordinators of store-operated Ca2+ entry. *Nature*. **499**, 238–242 (2013).
30. B. K. Deb, T. Pathak, G. Hasan, Store-independent modulation of Ca(2+) entry through Orai by Septin 7. *Nat. Commun.* **7**, 11751 (2016).
31. X. Liang, N. Zhang, H. Pan, J. Xie, W. Han, Development of Store-Operated Calcium Entry-Targeted Compounds in Cancer. *Front. Pharmacol.* **12**, 688244 (2021).
32. Q. Hu, W. J. Nelson, E. T. Spiliotis, Forchlorfenuron alters mammalian septin assembly, organization, and dynamics. *J. Biol. Chem.* **283**, 29563–29571 (2008).
33. F. Vallese *et al.*, An expanded palette of improved SPLICS reporters detects multiple organelle contacts in vitro and in vivo. *Nat. Commun.* **11**, 6069 (2020).
34. K. V. Kuchibhotla *et al.*, Abeta plaques lead to aberrant regulation of calcium homeostasis in vivo resulting in structural and functional disruption of neuronal networks. *Neuron*. **59**, 214–225 (2008).
35. Y. Yin *et al.*, Tau accumulation induces synaptic impairment and memory deficit by calcineurin-mediated inactivation of nuclear CaMKIV/CREB signaling. *Proc. Natl. Acad. Sci. USA.* **113**, E3773–81 (2016).
36. Y. Miao, A. Bhattarai, J. Wang, Ligand gaussian accelerated molecular dynamics (ligamd): characterization of ligand binding thermodynamics and kinetics. *J. Chem. Theory Comput.* **16**, 5526–5547 (2020).
37. D. C. Mendonça *et al.*, An atomic model for the human septin hexamer by cryo-EM. *J. Mol. Biol.* **433**, 167096 (2021).
38. J. Jumper *et al.*, Highly accurate protein structure prediction with AlphaFold. *Nature*. **596**, 583–589 (2021).
39. H. Takeuchi *et al.*, P301S mutant human tau transgenic mice manifest early symptoms of human tauopathies with dementia and altered sensorimotor gating. *PLoS One*. **6**, e21050 (2011).
40. A. H. Al-Nuaimi *et al.*, Robust EEG based biomarkers to detect alzheimer's disease. *Brain Sci.* **11** (2021), doi:10.3390/brainsci11081026.

41. C. Babiloni *et al.*, Measures of resting state EEG rhythms for clinical trials in Alzheimer's disease: Recommendations of an expert panel. *Alzheimers Dement.* (2021), doi:10.1002/alz.12311.
42. H. W. Querfurth, J. Jiang, J. D. Geiger, D. J. Selkoe, Caffeine stimulates amyloid beta-peptide release from beta-amyloid precursor protein-transfected HEK293 cells. *J. Neurochem.* **69**, 1580–1591 (1997).
43. H. W. Querfurth, D. J. Selkoe, Calcium ionophore increases amyloid beta peptide production by cultured cells. *Biochemistry*. **33**, 4550–4561 (1994).
44. N. Pierrot *et al.*, Calcium-mediated transient phosphorylation of tau and amyloid precursor protein followed by intraneuronal amyloid-beta accumulation. *J. Biol. Chem.* **281**, 39907–39914 (2006).
45. D. Xia *et al.*, Novel App knock-in mouse model shows key features of amyloid pathology and reveals profound metabolic dysregulation of microglia. *Mol. Neurodegener.* **17**, 41 (2022).
46. A. M. Pooler, E. C. Phillips, D. H. W. Lau, W. Noble, D. P. Hanger, Physiological release of endogenous tau is stimulated by neuronal activity. *EMBO Rep.* **14**, 389–394 (2013).
47. R. Praschberger *et al.*, Neuronal identity defines α-synuclein and tau toxicity. *Neuron*. **111**, 1577–1590.e11 (2023).
48. M. A. Busche, B. T. Hyman, Synergy between amyloid-β and tau in Alzheimer's disease. *Nat. Neurosci.* **23**, 1183–1193 (2020).
49. J. McDaid, S. Mustaly-Kalimi, G. E. Stutzmann, Ca2+ dyshomeostasis disrupts neuronal and synaptic function in alzheimer's disease. *Cells*. **9** (2020), doi:10.3390/cells9122655.
50. M. A. O'Neal, N. R. Stallings, J. S. Malter, Alzheimer's disease, dendritic spines, and calcineurin inhibitors: A new approach? *ACS Chem. Neurosci.* **9**, 1233–1234 (2018).
51. B. K. Deb, P. Chakraborty, R. Gopurappilly, G. Hasan, SEPT7 regulates Ca2+ entry through Orai channels in human neural progenitor cells and neurons. *Cell Calcium*. **90**, 102252 (2020).
52. B. K. Deb, G. Hasan, SEPT7-mediated regulation of Ca2+ entry through Orai channels requires other septin subunits. *Cytoskeleton (Hoboken)*. **76**, 104–114 (2019).
53. M. Ihara *et al.*, Association of the cytoskeletal GTP-binding protein Sept4/H5 with cytoplasmic inclusions found in Parkinson's disease and other synucleinopathies. *J. Biol. Chem.* **278**, 24095–24102 (2003).
54. Y. M. Gozal *et al.*, Aberrant septin 11 is associated with sporadic frontotemporal lobar degeneration. *Mol. Neurodegener.* **6**, 82 (2011).
55. G. Taglialatela, C. Rastellini, L. Cicalese, Reduced Incidence of Dementia in Solid Organ Transplant Patients Treated with Calcineurin Inhibitors. *J. Alzheimers Dis.* **47**, 329–333 (2015).